Energy Engineering

Tech Science Press

Doi:10.32604/ee.2026.074052

ARTICLE

Fault Reconfiguration Technology for Distribution Networks Considering Distributed Energy Output Forecasting

Honglian Gao[1], Qingsong Zhang[1], Zeming Chen[1], Lianchen Li[1], Quanhui Liu[1], Yuxiang Tian[1] and Xianfeng Xu[2,*]

[1]Guangdong Power Grid Co., Ltd. Guangzhou Power Supply Bureau, Guangzhou, China
[2]School of Energy and Electrical Engineering, Chang'an University, Xi'an, China

*Corresponding Author: Xianfeng Xu. Email: xxf_chd@163.com

Received: 30 September 2025; Accepted: 16 December 2025; Published: 30 August 2026

ABSTRACT: With the increasing penetration rate of distributed generators (DGs) in the distribution network, DGs with independent power supply capability provide strong support for distribution network fault recovery. Traditional fault reconfiguration methods often rely on static load priorities and fail to fully consider the time-varying dynamic characteristics of outage costs, resulting in shortcomings in the economy and adaptability of restoration strategies. To address this, this paper proposes a fault reconfiguration method that integrates day-ahead prediction and a dynamic load restoration set. Firstly, a Long Short-Term Memory network optimized by Variational Mode Decomposition and the Marine Predators Algorithm is used for the day-ahead prediction of DG output, providing a data foundation for rapid response upon fault occurrence. After a fault occurs, a time-varying dynamic load priority restoration set is constructed based on load outage cost analysis, comprehensively considering the load importance level and the decay characteristics of outage costs, forming an economy-oriented restoration objective. Furthermore, the islanding process and the main network reconfiguration process are unified into a single model, constructing a Mixed-Integer Second-Order Cone Programming model. This model is validated using the CPLEX solver on the IEEE 33-node and 69-node test systems. Simulation results show that, compared to traditional static reconfiguration methods, the proposed strategy not only ensures the continuous power supply to important loads but also significantly reduces user outage costs, achieving the synergistic optimization of power supply reliability and economy.

KEYWORDS: Distribution network; intelligent optimization algorithms; LSTM neural network; islanding formation; main grid reconfiguration; second-order cone programming (SOCP); distributed generation (DG)

1 Introduction

With the rapid development of China's power system, the requirements for power supply reliability and security in distribution networks have significantly increased [1]. Concurrently, the deployment of intelligent devices such as Distribution Automation Terminals (DATs) has substantially enhanced the detectability and controllability of distribution networks. This enables precise regulation of distribution grids and accurate switching control, laying the foundation for maximizing power restoration during faults through network reconfiguration and islanding formation [2].

Driven by China's "Dual Carbon" strategy, the integration of renewable energy sources in distribution networks continues to grow. The resulting active distribution networks make islanded power supply feasible for outage areas. However, traditional reconfiguration strategies have become inadequate for modern active distribution networks due to the incorporation of renewable energy. These strategies cannot support outage areas through islanding formation, necessitating in-depth research on network reconfiguration strategies for active distribution networks with DG during fault conditions.

During distribution network reconfiguration, speed requirements for post-fault processing often exist. Therefore, day-ahead prediction of DG output is essential. Current prediction methods in power systems primarily include statistical approaches and artificial intelligence (AI)-based predictive models. Among statistical methods, Exponential Smoothing [3] and Hidden Markov Models (HMMs) [4] are representative, yet such algorithms fail to capture certain features within the data. Consequently, AI-based predictive models [5] demonstrate superior practical utility due to their enhanced nonlinear fitting capabilities and comprehensive utilization of data details. Specifically, the Long Short-Term Memory (LSTM) network [6,7] enables accurate prediction for data with strong temporal patterns and has been extensively applied in time-dependent forecasting domains.

The essence of both main grid reconfiguration and islanding formation in distribution networks lies in adjusting the status of tie switches and sectionalizing switches to modify the network topology, thereby maximizing the restoration of power supply to outage areas. Numerous studies have addressed distribution network fault recovery and islanding formation. Reference [8] proposed an islanding strategy for outage areas based on the Knapsack Tree Algorithm but neglected dynamic variations in load demand and DG output. Reference [9] demonstrated the superiority of dynamic reconfiguration over static approaches. Reference [10] emphasized the necessity of considering dynamic load-DG interactions during islanding. Consequently, static reconfiguration methods prove inadequate for complex recovery requirements and may compromise solution feasibility. Furthermore, research indicates that outage cost per unit load decays exponentially over time [11], necessitating time-varying reconfiguration strategies.

Regarding the coordination of reconfiguration and islanding, existing literature typically treats them as separate processes. Reference [12] employed reconfiguration for power quality improvement, while Reference [13] developed an islanding-based recovery method using dynamic distributed linear programming to optimize island formation. Reference [14] proposed an improved Kruskal algorithm-based islanding scheme considering electrical distance and critical loads, coupled with a reconfiguration model to minimize active power losses and switching operations. These studies failed to integrate islanding with main grid reconfiguration during faults. Although Reference [15] combined both processes, it lacked in-depth analysis of outage cost implications.

In the optimization of reconfiguration strategies, scholars have employed various intelligent algorithms. For instance, reference [16] combined Particle Swarm Optimization with a plant growth simulation algorithm to reduce network losses, while reference [17] introduced the Seagull Optimization Algorithm to co-optimize reconfiguration and reactive power compensation. Furthermore, the coordinated optimization of reconfiguration and load control has garnered attention. Reference [18] proposed a reconfiguration model integrating a minimum spanning tree algorithm with an improved genetic algorithm to optimize load shedding. However, few of the aforementioned studies have sufficiently considered the new challenges introduced by distributed generation—such as harmonic pollution, as highlighted in reference [19]—or have deeply integrated the processes of islanding and main network reconfiguration under fault conditions. Simultaneously, as emphasized in reference [20], precise switch configuration is crucial for implementing load management, which further underscores the importance of comprehensively considering switch operations and load priorities during reconfiguration.

In summary, the core contribution of this paper lies in proposing a distribution network reconfiguration method that accounts for dynamic cost variations, aiming to achieve cost-economic restoration. Building upon the characteristic of time-decaying outage costs, the approach rapidly establishes a dynamically updated load priority recovery set based on day-ahead forecasts of distributed energy output, forming the cornerstone of the reconfiguration strategy. By integrating islanding formation with main grid reconfiguration during fault conditions, network reconfiguration serves as the technical means to achieve the ultimate objective of optimal load and cost recovery. While reconfiguration guides the system's transition from fault state to power supply restoration, the economically reliable recovery of loads constitutes the overarching optimization goal that fundamentally governs the generation and selection of reconfiguration schemes. This framework ultimately accomplishes a comprehensive fault self-healing technology that simultaneously considers both cost and load importance.

Key innovations include:

1. Enhancing traditional LSTM networks via intelligent optimization algorithms for domain-specific adaptability;
2. Proposing a novel time-varying load priority recovery set incorporating decaying outage costs, it provides a reliable objective for post-fault management in distribution networks. The dynamic restoration set generated by this method serves as the core decision-making benchmark for reconfiguration strategies, enabling the restoration process to holistically balance load importance with power supply restoration economics;
3. Reducing computational burden through integrated islanding-reconfiguration coordination, providing an efficient solution approach for the proposed dynamic cost-based reconfiguration method.

2 LSTM-Based DG Output Forecasting Utilizing VMD and Intelligent Optimization Algorithms

In active distribution network fault reconfiguration, process immediacy is crucial. Consequently, initiating reconfiguration solely based on real-time DG output data after fault occurrence often prolongs response time. To address this limitation, this study employs a Variational Mode Decomposition (VMD)-enhanced LSTM network with intelligent optimization algorithms for day-ahead wind-solar output forecasting. This approach obtains predicted DG output data in advance, enabling immediate fault reconfiguration using forecasted data during outages.

2.1 Fundamental Principles of VMD

Variational Mode Decomposition (VMD), an adaptive signal decomposition method, achieves effective frequency-domain partitioning and separation of signal components. Its fundamental process involves iteratively solving a variational model to determine the center frequencies and finite bandwidths of intrinsic mode functions (IMFs).

The mathematical expression for the k-th order IMF is given by:

$$F_u = A_k(t)\cos(\phi_k(t)), \tag{1}$$

$$F_\omega = \phi_k^{'}(t) = \frac{\mathrm{d}\phi_k(t)}{\mathrm{d}t} \tag{2}$$

In the equation, F_u is the $u_k(t)$ function, $A_k(t)$ is the $u_k(t)$ instantaneous amplitude, $k = 1, 2, \ldots, K$, F_ω is the $\omega_k(t)$ function, $\omega_k(t)$ is the center frequency of $u_k(t)$, $\phi_k(t)$ is the non-monotonically decreasing phase function.

By Hilbert transform obtaining the analytic signal of $u_k(t)$, thus acquiring the unilateral spectrum:

$$\left[\delta(t) + \frac{h}{\pi t}\right] * u_k(t) \tag{3}$$

In the equation, $\delta(t)$ is the impulse function, h represents this time instant.

By adjusting the center frequency $\omega_k(t)$ of each $u_k(t)$, and mixing with the unilateral spectrum in Eq. (3), obtaining the baseband signal:

$$\left[\left(\delta\left(t\right)+\frac{h}{\pi t}\right)*u_k\left(t\right)\right]\mathrm{e}^{-j\omega_k t} \tag{4}$$

By calculating the gradient of the demodulated signal, obtaining the bandwidth of the demodulated signal to establish the constrained variational model expression:

$$\min_{\{\mu_k\},\{\omega_k\}}\left\{\sum_{k=1}^{K}\left\|\partial_t\left[\left(\delta\left(t\right)+\frac{h}{\pi t}\right)*u_k\left(t\right)\right]\mathrm{e}^{-j\omega_k t}\right\|_2^2\right\}, \tag{5}$$

$$\text{s.t.}\sum_{k=1}^{K}u_k\left(t\right)=f \tag{6}$$

In the equation, f is expressed as $f(t)$, representing the input signal, $\{\mu_k\}=\{\mu_1,\mu_2,\ldots,\mu_k\}$, are k mode components, $\{\omega_k\}=\{\omega_1,\omega_2,\ldots,\omega_k\}$, are the frequency centers corresponding to the k mode components. To convert it into an unconstrained variational problem, introducing a quadratic penalty factor and Lagrange multiplier, thereby obtaining the augmented Lagrangian expression:

$$\begin{aligned}L\left(\{\mu_k\},\{\omega_k\},\lambda\right)=\alpha\sum_k\left\|\partial_t\left[\left(\delta\left(t\right)+\frac{h}{\pi t}\right)*u_k\left(t\right)\right]\mathrm{e}^{-j\omega_k t}\right\|_2^2\\+\left\|f\left(t\right)-\sum_k u_k\left(t\right)\right\|_2^2+\left\langle\lambda\left(t\right)f\left(t\right)-\sum_k u_k\left(t\right)\right\rangle\end{aligned} \tag{7}$$

In the equation, α is the penalty factor, $\lambda(t)$ is the Lagrange multiplier, the operator "⟨⟩" represents the inner product.

$$\sum_{k=1}^{k}\frac{\|\hat{u}_k^{n+1}-\hat{u}_k^{n}\|_2^2}{\|\hat{u}_k^{n}\|_2^2}<\varepsilon \tag{8}$$

In the equation, ε is the convergence tolerance.

Using the multiplier alternating direction method continuously alternately updating $\hat{u}_k^{n+1}$, and after satisfying Eq. (8), immediately stopping iteration, obtaining k mode component values.

2.2 Fundamental Principles of the Marine Predators Algorithm (MPA)

The MPA, as a novel metaheuristic optimization algorithm, exhibits superior performance in solving complex problems due to its rapid convergence, high accuracy, and strong stability. It emulates marine predators' foraging strategies based on Lévy and Brownian motions, along with optimal encounter strategies for biological individual interactions.

The MPA procedure comprises four phases:

1. Initialization: Randomly initializes prey positions, representing algorithm initialization.
2. Optimization: Predators select strategies based on prey behavior, enabling balanced local and global search.
3. Fish Aggregating Devices (FADs) and Eddy Effect: Addresses local optima traps. Predators employ long-jump steps to escape eddies, preventing premature convergence.

4. Population Update: Implements a 50/50 predator-prey update strategy, enhancing global search while accelerating local search through FAD-induced vortex effects.

Additionally, MPA's memory mechanism retains optimal solutions, outperforming comparable algorithms. The mathematical formulation is expressed as:

2.2.1 Initialization

Initialize the Prey matrix, namely the prey matrix:

$$X_{ij} = X_{\min} + rand\left(X_{\max} - X_{\min}\right) \tag{9}$$

In the equation, X_{min} is the lower bound of the search space, X_{max} is the upper bound of the search space, $rand()$ represents a random vector, taking values between 0 and 1.

Obtain the Prey matrix:

$$Prey = \begin{bmatrix} X_{1,1} & \dots & X_{1,d} \\ \vdots & \vdots & \vdots \\ X_{n,1} & \dots & X_{n,d} \end{bmatrix} \tag{10}$$

In the equation, n denotes the population size, and d represents the dimension of the solution.

The Elite matrix maintains the same dimensionality as the Prey matrix. At the end of each iteration, the predators in the current iteration are compared with the top predators from the previous iteration, and the Elite matrix is updated with the superior predators.

$$Elite = \begin{bmatrix} X^I_{1,1} & \dots & X^I_{1,d} \\ \vdots & \vdots & \vdots \\ X^I_{n,1} & \dots & X^I_{n,d} \end{bmatrix} \tag{11}$$

2.2.2 Optimization

Optimization process is divided into three sequential phases, where the dynamic interplay between predator-prey velocity ratios governs the simultaneous simulation of both predator and prey movement behaviors. These operational phases are defined as follows:

Initialization Phase: When the prey's instantaneous velocity exceeds the predator's velocity (i.e., high prey-to-predator velocity ratio), the prey population exhibits Brownian motion-inspired exploratory patterns. During this phase:

$$\begin{cases} stepsize_i = R_B \otimes \left(Elite_i - R_B \otimes \Pr ey_i\right) \\ \Pr ey_i = \Pr ey_i + P \cdot R \otimes stepsize_i \end{cases} \quad i = 1, 2 \dots n \quad Iter < \frac{1}{3} Iter_{\max} \tag{12}$$

In the equation, $stepsize_i$ represents the movement step size, R_B represents a random vector based on the normal distribution of Brownian motion, $\otimes$ is the entry-wise multiplication operator, P is an arbitrary constant that can be modified according to actual conditions, R is a random vector taking values between 0 and 1, n represents the population size, $Iter$ represents the current iteration count, $Iter_{max}$ represents the maximum iteration count.

Intermediate Optimization Phase: When predator and prey velocities reach approximate parity, the prey population employs Lévy flights to conduct local exploitation, while the predator population utilizes Brownian walks to perform global exploration.

$$\begin{cases} stepsize_i = R_L \otimes (Elite_i - R_L \otimes \Pr ey_i) \\ \Pr ey_i = \Pr ey_i + P \cdot R \otimes stepsize_i \end{cases} \quad i = 1, 2 \ldots n/2 \ \frac{1}{3} Iter_{\max} < Iter < \frac{2}{3} Iter_{\max}, \tag{13}$$

$$\begin{cases} stepsize_i = R_B \otimes (R_B \otimes Elite_i - \Pr ey_i) \\ \Pr ey_i = Elite_i + P \cdot CF \otimes stepsize_i \end{cases} \quad i = n/2 \ldots, n \ \frac{1}{3} Iter_{\max} < Iter < \frac{2}{3} Iter_{\max} \tag{14}$$

In the equation, R_L denotes a random vector following a Lévy distribution. $CF = (1 - Iter/Itermax)^{2Iter/Itermax}$ denotes the adaptive parameter that regulates the predator's movement step size.

Late Optimization Phase: when the predator's velocity exceeds that of the prey, the optimization algorithm enters a state of intensive exploitation. During this phase, predator agents employ Lévy flights to execute targeted pursuit behaviors.

$$\begin{cases} stepsize_i = R_L \otimes (R_L \otimes Elite_i - \Pr ey_i) \\ \Pr ey_i = Elite_i + P \cdot CF \otimes stepsize_i \end{cases} \quad i = 1, 2 \ldots n \quad Iter > \frac{2}{3} Max\_Iter \tag{15}$$

2.2.3 FADs and Eddy Effect

$$\Pr ey_i = \begin{cases} \Pr ey_i + CF\left[X_{\min} + R \otimes (X_{\max} - X_{\min})\right] \otimes Ur \leq FADs \\ \Pr ey_i + \left[FADs\,(1-r) + r\right](\Pr ey_{r1} - \Pr ey_{r2})\, r > FADs \end{cases} \tag{16}$$

In the equation, *FADs* represents the degree to which fish aggregation devices affect the optimization progress, U denotes a binary vector, r is a random number between 0 and 1, and r_1 and r_2 are random indices of the prey matrix.

2.2.4 Population Update

This process updates the Elite Matrix. Through the comparison of the individual fitness of the predator matrix and the elite matrix in this iteration, if it is better than the elite matrix, it will be replaced until the algorithm requirements are met.

2.3 LSTM Neural Network

As an improved recurrent neural network (RNN), it can effectively solve the prediction time series with long intervals in recurrent neural networks, and its structure is shown in Fig. 1.

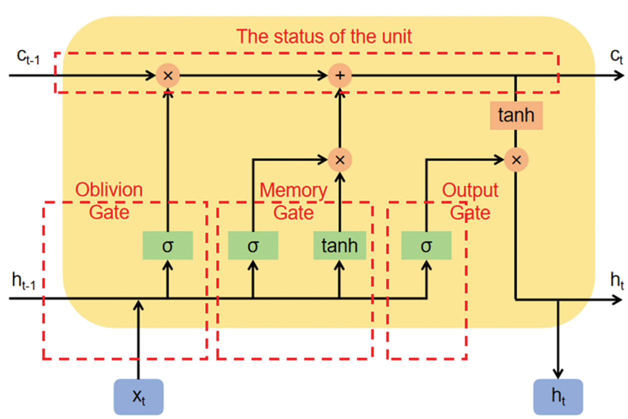

Figure 1: Schematic illustration of the LSTM structure

In the figure, the output h_t of the LSTM neural network will be determined by the output h_{t-1} at the previous time, the unit state c_{t-1} at the previous time, and the input x_t at this time.

3 Typical Energy Storage Device Output Model

As a critical component in active distribution networks, energy storage devices play a pivotal role in fault reconfiguration technology for such systems. Serving as the power source supporting reliable power restoration in de-energized areas, research on the output performance of energy storage devices directly impacts system reliability and the effectiveness of reconfiguration strategies. Consequently, prior to implementing unified reconfiguration of active distribution networks under fault conditions, this paper first conducts a comprehensive analysis of energy storage device output characteristics to establish their operational constraints during fault scenarios. Building upon this foundation, this section focuses on establishing an energy storage technology modeling framework and developing an integrated output model for distributed power sources, thereby providing essential energy support for the formulation of distribution network fault reconfiguration strategies.

3.1 Energy Storage System Output Model

Unlike wind and photovoltaic power, the output model of energy storage systems is relatively complex. Therefore, the primary consideration is to limit its output range through operational constraints. In this paper, both capacity and power limitations are taken into account comprehensively. Additionally, to consider the lifespan of energy storage equipment, simultaneous charging and discharging behaviors are not allowed.

3.1.1 Charging and Discharging Constraints

$$E_{ch} + E_f \leq 1, \tag{17}$$

this equation is used to restrict the charging and discharging states of energy storage. Specifically, when E_{ch} is 1, it indicates that the energy storage device is charging; when E_f is 1, it indicates that the energy storage device is discharging. This constraint enforces that the sum of E_{ch} and E_f must not exceed 1, mathematically ensuring that both states cannot be 1 simultaneously, thereby implementing a hard constraint against the prohibited behavior of "simultaneous charging and discharging." This model establishes the foundation for subsequent development of a safe operational framework for the energy storage system.

3.1.2 Energy Storage Device Charging Model

Although the possibility of energy storage devices remaining in a charging state during fault conditions in the distribution network is very low, it is still necessary to model this scenario to ensure the overall validity of the model.

$$E_{\Delta t} = E_0 + \int_0^{\Delta t} P_{ch,t} \alpha_1 dt, P_{ch,t} \leq P_{ch,\max} \tag{18}$$

In the equation, E_0 represents the initial energy level of the energy storage device, $E_{\Delta t}$ represents the energy level of the device after a time interval of Δt, $P_{ch,t}$ represents the charging power of the device at time t, α_1 represents the charging efficiency of the device, $P_{ch,max}$ represents the maximum charging power of the device.

3.1.3 Energy Storage Device Discharging Model

$$E_{\Delta t} = E_0 - \int_0^{\Delta t} P_{f,t}/\alpha_2 dt, P_{f,t} \leq P_{f,\max} \tag{19}$$

In the equation, E_0 represents the initial energy level of the energy storage device, $E_{\Delta t}$ represents the energy level of the device after a time interval of Δt, $P_{f,t}$ represents the discharging power of the device at time t, α_1 represents the charging efficiency of the device, $P_{f,max}$ represents the maximum discharging power of the device.

3.1.4 State of Charge of Energy Storage Device and Its Constraints

In practical applications, energy storage systems often use the State of Charge (SOC) to indicate their remaining capacity. This paper adopts a dynamic SOC update model widely used in hybrid energy storage systems, which performs recursive calculations of the SOC based on the operating mode of the energy storage device.

During charging ($P_{E,t} \geq 0$):

$$SOC_t = SOC_{t-1} + \frac{P_{E,t} \cdot t \cdot \eta_{ch}}{E_N} \tag{20}$$

During discharging ($P_{E,t} < 0$):

$$SOC_t = SOC_{t-1} + \frac{P_{E,t} \cdot \Delta t}{\eta_{dis} \cdot E_N} \tag{21}$$

In the equation, SOC_t and SOC_{t-1} represent the state of charge at time t and $t-1$ respectively; $P_{E,t}$ denotes the charging/discharging power of the energy storage device at time t; η_{ch} and η_{dis} represent the charging efficiency and discharging efficiency of the energy storage device respectively; E_N is the rated capacity of the energy storage device; and Δt is the time interval.

Meanwhile, to ensure the safe operation of the energy storage device, overcharging and over-discharging are not allowed. The safety constraints for the energy storage device are expressed in Eq. (22) as follows:

$$SOC_{\min} \leq SOC_{t_0+\Delta t} \leq SOC_{\max} \tag{22}$$

In the equation, SOC_{min} represents the minimum SOC of the energy storage device, and SOC_{max} represents the maximum SOC of the energy storage device.

3.2 Integrated Output Model for Distributed Power Sources

In practical applications, energy storage devices are often combined with photovoltaic panels and wind turbines to obtain a relatively stable power output, providing strong support for the reconfiguration process of distribution networks, especially in the division of islands. The integrated output of distributed power sources is shown in Eq. (23):

$$P_{DG} = P_f + P_g + P_E \tag{23}$$

In the equation, P_{DG} represents the integrated output of distributed power sources, P_f represents the output of wind turbines, P_g represents the output of photovoltaic units, and P_E represents the output of the energy storage system.

The output of distributed power sources used in the fault reconfiguration process of distribution networks in this paper is derived from this equation.

4 Unified Model for Fault Reconfiguration and Islanding Partition in Active Distribution Networks

During the operation of distribution networks, faults in the upstream grid may result in the loss of main power supply in some areas. To ensure continuous power supply to these areas, distribution network reconfiguration strategies have emerged. Distribution network reconfiguration aims to form self-sufficient power islands in fault areas during grid faults by reasonably scheduling the power of distributed power sources and energy storage devices, and utilizing interruptible loads, thereby reducing user outage losses and enhancing the reliability of power supply in distribution networks. This chapter will explore the research content of fault reconfigur-ation and islanding partition models for active distribution networks, including the establishment of objective functions for network reconfiguration, constraint conditions for network reconfiguration, and adaptation to the CPLEX solver, providing theoretical support and practical guidance for the islanding operation of actual distribution networks.

4.1 Priority Restoration Set for Loads That Vary over Time

When faults occur in distribution network lines, the strategies for reconfiguration and islanding partition of active distribution networks become particularly important. The main objective during this fault handling phase is to, after a fault in the distribution network line, reasonably adjust the grid structure so that the main grid can support as many power-loss nodes as possible, and to rationally allocate distributed power sources within the distribution area to form self-sufficient island regions for load nodes that cannot be connected to the distribution network due to the fault. This ensures that critical loads avoid power loss, reduces outage costs for users, and thus enhances the safety and reliability of power supply in distribution networks. Therefore, this paper prioritizes the establishment of a priority restoration set for loads that vary over time. This strategy complies with the requirements of IEEE 1547-2003 for utilizing islanding operation of distributed power sources to improve power supply reliability. It also provides strong support for the current situation where modern active distribution networks account for an increasing proportion, and is an important means to ensure the safety of power supply.

For power-loss load areas that cannot be connected to the main grid, after the island is formed, the power supply that was originally uniformly dispatched by the upstream grid will be shared by the distributed power sources and energy storage devices within the island. This transition requires precise calculation and balancing of power supply and demand within the island to ensure its stable operation. Therefore, fault reconfiguration in distribution networks is not merely a simple

process of load shedding and power source connection; it is a complex process involving multiple aspects of the power system and requiring comprehensive consideration of various factors.

1) Load power loss considering load importance weight

The classification of power load levels is a crucial aspect in power systems. Based on the importance of the load and the impact of power interruption, power loads can be divided into three levels: Level I load, Level II load, and Level III load.

Level I load refers to the load that, once its power supply is interrupted, will cause significant losses to personal safety, economic development, and normal order. For example, all loads related to life safety, commercial centers in major cities, and important public places belong to Level I load.

Level II load refers to the load where power interruption would cause considerable losses to social economy and normal order. These loads are typically important loads for local government departments, large and medium-sized enterprises, hospitals, schools, and so on.

Level III load refers to the load where power interruption would not have a significant impact on social economy and normal order. These loads are usually general loads found in small businesses, rural areas, remote regions, and so forth. The classification criteria for different load levels are summarized in Table 1.

Table 1: Load classification

Importance level	Classification conditions
I	No power interruption allowed under any circumstances
II	Minimize power outages
III	Can be cut in shortage

Based on different load levels, power systems will adopt different power supply measures to ensure the reliability and safety of loads at various levels. In the context of islanding partition, load levels will be reflected in the weight assigned to each node.

Based on this, the evaluation elements for the priority restoration set based on load importance levels can be derived, and its expression is:

$$f_1 = \min \sum_{i=1}^{n} \omega_i P_{L,i} x_i \tag{24}$$

In the equation, x_i epresents the proportion of load outage, where $x_i = 0$ indicates complete restoration of power supply to the outage load, and conversely $x_i = 1$; $P_{L,i}$ represents the active power of the load at node i; ω_{i} represents the load weight coefficient of node i, with values of 100 for Level I load, 10 for Level II load, and 1 for Level III load.

From the above Eq. (24), it can be seen that when partitioning islands, nodes with greater weights will be prioritized for inclusion within the island. However, when the weight coefficients of two outage nodes are equal, which outage node should be included in the island? At this point, the outage cost of the two nodes needs to be considered, with the node having the higher cost being prioritized for inclusion in the island.

2) Time-varying load outage cost

When certain areas of the active distribution network are operating as islands and the power supply capacity from distributed generation and energy storage is insufficient, some loads need to be shed to maintain supply-demand balance. In the process of load shedding, priority can be given to interrupting loads with lower load weights and smaller outage losses among the outage nodes. If the power supply capacity remains insufficient, loads of higher importance will be shed based on their load importance levels and the degree of outage losses.

Due to the significant social losses caused by power outages to Category I loads, it is necessary to ensure continuous power supply to Category I loads during upper-level grid faults, strive to maintain continuous power supply to Category II loads, and allow power outages to Category III loads during island operation.

From the trend of power outage losses over time, most electric power users exhibit a nonlinear positive correlation between outage losses and outage duration, characterized by a steep slope initially and a gentler slope later on. This is summarized in the user loss diagram shown in Fig. 1, where the red curve represents the user loss curve over time, and the green bars represent user losses per unit of time.

Traditional load priority restoration strategies predominantly rely on static load importance classifications, failing to adequately account for the time-varying attenuation characteristics of outage costs. Therefore, this paper proposes a user loss attenuation model that varies with outage duration. It not only considers the static importance of loads but also introduces a dynamic dimension of cost. This model will make the distribution network more inclined to continue supplying power to loads with the least outage in the previous period during island partitioning, the distribution network tends to prioritize continuous power supply to loads that experienced the least outage duration in the previous time period, in order to reduce the total user losses during faults in the active distribution network. The expression is given in Eq. (25):

$$f_2 = \min \sum_{i=1}^{n} C_i P_{L,i} x_i \gamma \tag{25}$$

In the equation, C_i represents the initial user outage loss cost at node i; γ represents the loss attenuation constant, which corresponds to the change in area per unit time of the bar chart shown in Fig. 2.

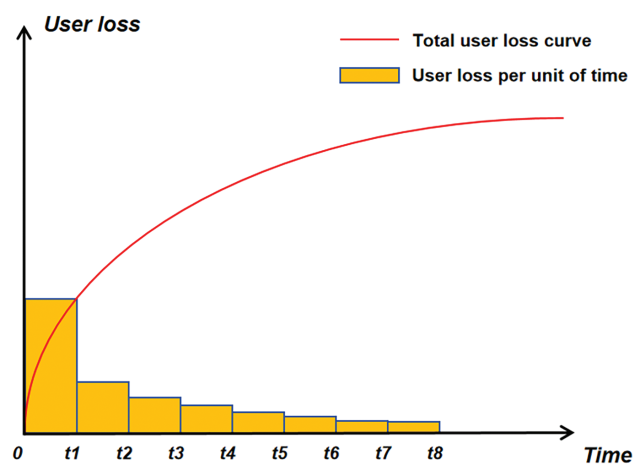

Figure 2: User losses over time

While minimizing the total outage cost, the proposed model also strives to maximize the power supply restoration. The underlying logic is that by accurately characterizing the time-varying nature of outage costs, the optimization algorithm can prioritize the restoration of loads that yield the highest "cost savings" per unit of available power capacity at any given moment. This economically-guided restoration strategy essentially drives the system towards islanding and reconfiguration that achieves the largest possible supply scope and the highest comprehensive benefit. Consequently, it simultaneously reduces the total cost while maximizing the amount of restored de-energized load.

This time-varying cost model serves as the core mechanism for minimizing total outage losses post-fault. Its optimization principle lies in transforming cost assessment from static to dynamic through the introduction of the temporal dimension, enabling the reconfiguration strategy to precisely respond to the attenuation characteristics of outage losses. As illustrated in Fig. 2, due to the nonlinear decay of user loss curves, prioritizing the restoration of loads at stages with higher loss rates during any decision-making moment allows the same power supply capacity to achieve greater cost reduction benefits. This systematically guides the reconfiguration process toward global loss minimization.

Next, we discuss the impact of this model on island partitioning for power outage areas in distribution networks.

As shown in Fig. 3, when DG is connected to the distribution network at node a, and nodes i and j are the outage nodes during a fault, if the equivalent loads f_{1i} and f_{1j} are equal.

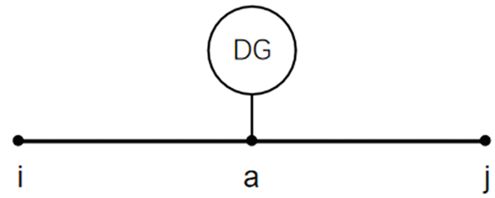

Figure 3: Analysis model for cost losses in distribution networks

Both nodes could potentially be included in an island without affecting the overall f_1, ignoring the impact of user outage costs. However, if the impact of user outage costs is taken into account, since the user outage cost $f_{2i} < f_{2j}$, the outage load at node *i* should be prioritized for inclusion in the island. This approach can effectively reduce the user outage costs within the island.

3) Load power loss considering load importance weight

In traditional islanding strategies, a fundamental assumption is typically made: each independently operating island contains only one distributed generator (DG) as the primary supporting power source. This assumption simplifies the complexity of control and protection, ensuring the stability of islanded operation. However, in actual distribution network fault scenarios, the location of faults and the distribution of outage areas are random, which may result in multiple DGs being isolated within the same outage area. If the "one-island-one-source" principle is strictly followed, forcing multiple interconnectable DGs to be divided into smaller islands may lead to unnecessary load shedding within the power supply range of individual DGs due to capacity limitations, thereby reducing the system's power supply restoration capability.

Therefore, the model proposed in this paper does not enforce the "one-island-one-source" rule. Instead, through optimized search, it allows for the formation of multi-source islands. The fundamental objective is to restore as much of the outage load as possible, particularly high-priority loads, while ensuring the safe operation of the system, thereby achieving comprehensive minimization of outage costs and load losses.

4.2 Construction of the Objective Function for Island Partitioning Based on the Load Priority Restoration Set

After analyzing the weight of load importance levels and the cost weight of outage load losses, we can obtain the objective function for island partitioning based on the load priority restoration set. This function will comprehensively adjust the load priority restoration set based on the load outage duration and outage ratio, while ensuring that the weights based on load importance levels remain unaffected.

The comprehensive objective function for distribution network reconfiguration is shown in Eq. (26):

$$f = \min\left(\beta_1 f_1 + \beta_2 f_2\right) \tag{26}$$

In the equation, β_1 and β_2 are the weights for the two parts of the load priority restoration set, with $\beta_1 + \beta_2 = 1$. In this paper, both β_1 and β_2 are set to 0.5.

1) Constraint Conditions

An active distribution network contains active equipment such as wind turbines, photovoltaics, and energy storage. When a fault in the upper-level grid necessitates distribution network reconfiguration and island partitioning, the primary operational constraint that needs to be satisfied is the system power flow constraint.

Distribution network reconfiguration must satisfy the radial structure constraint, meaning the reconfigured network must contain no loops while ensuring all energized nodes remain connected to the power source. This constraint forms the basis for simplifying protection settings, avoiding circulating currents, and ensuring stable operation in distribution networks. From a graph theory perspective, a radial network constitutes a spanning tree structure. For a connected energized area with n nodes, the number of energized branches must be exactly n − 1. This ensures the existence of a unique path between any two nodes. Mathematically, this constraint is enforced by limiting the total number of closed branches through Eq. (27) to guarantee loop-free operation.

$$g_m \in G_M \tag{27}$$

In this paper, the DistFlow power flow constraint suitable for radial networks is used, a framework specifically designed for accurate power flow calculation in radial distribution networks. Based on branch flow theory, this model directly formulates the relationship between power flow between nodes and voltage drop, circumventing the complexity inherent in traditional Newton-Raphson methods designed for whole-network power flow calculations. Its core advantage lies in using branch power and the square of node voltages as variables, which gives the constructed power balance and voltage equations clear physical meaning and a tractable mathematical form within radial networks, making them highly suitable for embedding into optimization models. With a 0–1 variable $Z_{i,j}^t$ indicating whether a line is disconnected or not. This enhances the applicability of the flexible topology transformation characteristic during the fault restoration process of the distribution network with the DistFlow power flow constraint. Additionally, the direction from the initial node to the terminal node in the branch information is defined as positive.

To enhance the mathematical rigor and optimization efficiency of the model, and in line with common practices in the DistFlow framework, the squares of voltage and current are introduced as optimization variables, defined as:

$$\overline{U}_i = V_i^2 \tag{28}$$

$$\overline{I}_{ij} = I_{ij}^2 \tag{29}$$

In the power balance equations, the line loss (I^2R) can be directly expressed as $\bar{I}_{ij} \times R$, thereby avoiding the nonlinearity inherent in the current variable I itself. Moreover, the original power-voltage-current relationship is non-convex. By adopting V^2 and I^2 as variables, the non-convex constraints can be naturally relaxed into a convex second-order cone formulation. This transformation enables efficient determination of the global optimum or high-quality feasible solutions using solvers such as CPLEX.

The constraint equations based on the DistFlow power flow constraint are shown in Eqs. (30)–(34):

$$\sum P_{i,j}^t - \sum P_{j,k}^t - \sum r_{i,j}\overline{I}_{i,j}^t = \left(P_{j,L}^t - P_{j,\mathrm{DG}}^t\right), \tag{30}$$

$$\sum Q_{i,j}^t - \sum Q_{j,k}^t - \sum x_{i,j}\overline{I}_{i,j}^t = \left(Q_{j,L}^t - Q_{j,\mathrm{DG}}^t\right) \tag{31}$$

In the equations, $\sum P_{i,j}^t, \sum P_{j,k}^t, P_{j,L}^t, P_{j,DG}^t$ represent the total injected active power, total outgoing active power, node active load, and total active power output of DG at node j in time period t, respectively; $\sum Q_{i,j}^t, \sum Q_{j,k}^t, Q_{j,L}^t, Q_{j,DG}^t$ represent the total injected reactive power, total outgoing reactive power, predicted reactive load, and total reactive power output of DG at node j in time period t, respectively; $\overline{I}_{i,j}^t$

represents the squared current term on the branch from node i to node j in time period t; $\sum r_{i,j}\overline{I}_{i,j}^{t}$, $\sum x_{i,j}\overline{I}_{i,j}^{t}$ represent the total active and reactive line losses injected into the line at node j at time t, respectively.

The big M method is a mathematical approach commonly used to solve optimization problems containing discrete variables. Its core concept involves introducing a sufficiently large constant M to transform logical constraints into linear inequalities, thereby adapting them to the requirements of mixed-integer programming solvers. The use of the big M method enables the line voltage drop balance equations to be applicable to complex distribution networks with variable topologies. The constructed line voltage drop balance equations are shown in Eqs. (30)–(32).

$$m_{i,j} = \left(1 - Z_{i,j}^{t}\right) M, \tag{32}$$

$$\overline{U}_{i}^{t} - \overline{U}_{j}^{t} \leq m_{i,j} + 2\left(r_{i,j}P_{i,j}^{t} + x_{i,j}Q_{i,j}^{t}\right) - \left(r_{i,j}^{2} + x_{i,j}^{2}\right)\frac{\left(P_{i,j}^{t}\right)^{2} + \left(Q_{i,j}^{t}\right)^{2}}{\overline{U}_{i}^{t}}, \tag{33}$$

$$\overline{U}_{i}^{t} - \overline{U}_{j}^{t} \geq -m_{i,j} + 2\left(r_{i,j}P_{i,j}^{t} + x_{i,j}Q_{i,j}^{t}\right) - \left(r_{i,j}^{2} + x_{i,j}^{2}\right)\frac{\left(P_{i,j}^{t}\right)^{2} + \left(Q_{i,j}^{t}\right)^{2}}{\overline{U}_{i}^{t}} \tag{34}$$

In the equation, M represents a very large constant; $\overline{U}_{i}^{t}$ represent the square of the voltage at node i in time period t; $r_{i,j}$, $x_{i,j}$ represent the resistance and reactance of the line from node i to node j; $P_{i,j}^{t}$, $Q_{i,j}^{t}$ represent the active and reactive power injected from node i to node j in time period t.

In addition, to ensure the safe and stable operation of the distribution network, the parameters of each line in the distribution network during a fault need to satisfy the capacity and voltage constraints shown in Eqs. (35) and (36).

$$\begin{cases} -Z_{i,j}^{t}M \leq P_{i,j}^{t} \leq Z_{i,j}^{t}M \\ -Z_{i,j}^{t}M \leq Q_{i,j}^{t} \leq Z_{i,j}^{t}M & \forall\,(i,j) \\ \left(P_{i,j}^{t}\right)^{2} + \left(Q_{i,j}^{t}\right)^{2} \leq {S_{\max}}^{2} \end{cases}, \tag{35}$$

$$(1-y)^{2}U_{\mathrm{N}}^{2} \leq \overline{U}_{i}^{t} \leq (1+y)^{2}U_{\mathrm{N}}^{2} \tag{36}$$

In these two equations, Eq. (33) represents the capacity constraint for the branches of the distribution network, and Eq. (34) represents the voltage deviation constraint for the nodes of the distribution network; S_{max} represents the maximum allowable capacity of the line, U_{N}^{2} represents the square of the rated voltage at the load node, and y represents the allowable degree of voltage deviation.

2) Second-Order Cone Relaxation Suitable for CPLEX Solver

Due to the inability of the CPLEX solver to solve non-convex problems, it is necessary to perform second-order cone relaxation on the quadratic constraints relating voltage, current, and power mentioned earlier. This is shown in Eq. (37):

$$\left\| \begin{matrix} 2P_{i,j}^{t} \\ 2Q_{i,j}^{t} \\ \overline{I}_{i,j}^{t} - \overline{U}_{i,j}^{t} \end{matrix} \right\|_{2} \leq \overline{I}_{i,j}^{t} + \overline{U}_{i,j}^{t} \tag{37}$$

The meanings of the physical quantities contained in the equation remain consistent with those mentioned earlier.

3) Flowchart of the Distribution Network Reconfiguration Process Aimed at Minimizing Outage Load and Cost Losses

The flowchart of the distribution network reconfiguration process aimed at minimizing outage load and cost losses is shown in Fig. 4:

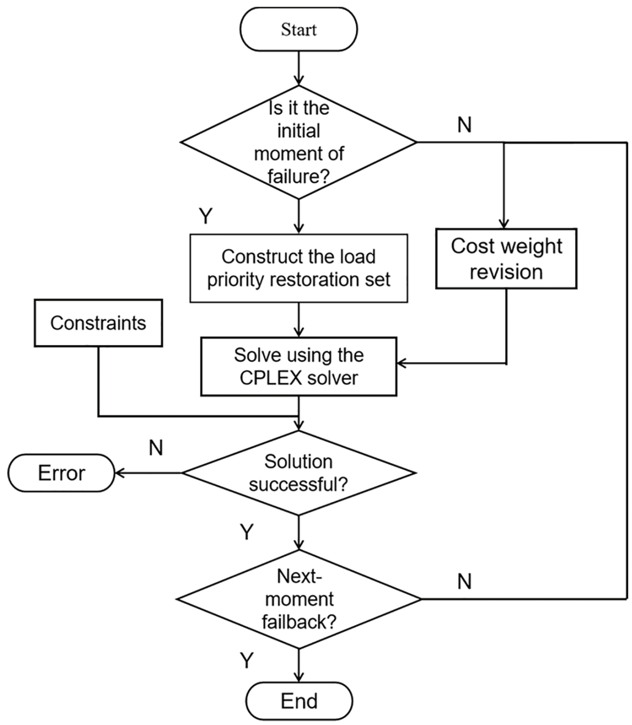

Figure 4: Flowchart

The fault reconfiguration strategy process for active distribution networks can be summarized as follows:

1. At the initial fault moment, establish a distribution network reconfiguration framework using the load priority restoration set as the optimization objective and the aforementioned constraints as operational limits.
2. Solve the distribution network reconfiguration framework to obtain the optimal load priority restoration set under comprehensive evaluation metrics of load power loss and outage cost. Control line switch states through distribution network reconfiguration to restore power to nodes within the optimal load priority restoration set, thereby achieving the reconfiguration objective.
3. If the fault is resolved in the next time step, terminate the operation. Otherwise, update the outage cost evaluation metric according to Eq. (25), refresh the load priority restoration set, and return to Step 2 to continue the solution process.

5 Case Analysis

5.1 The Day-Ahead Output Forecast Part

Since the form of output prediction of distributed energy resources is very similar, the experimental part will mainly predict photovoltaic power generation, and the VMD-MPA-LSTM method mentioned above will be used as the prediction method.

5.1.1 Parameter Settings

To validate the performance of the proposed VMD-MPA-LSTM method in photovoltaic power generation forecasting, it is essential to configure the key parameters of the prediction model. The forecasting inputs are selected based on critical environmental factors influencing PV output, including solar irradiance, ambient temperature, atmospheric pressure, and humidity. Among these, solar irradiance serves as the most direct and fundamental driver of photovoltaic power generation and has been widely adopted as the primary input for prediction models in relevant studies [21]. The parameter settings of the MPA optimizer, aimed at efficiently searching for the optimal hyperparameters of the LSTM network, are summarized in the table below.

Table 2 lists the parameters.

Table 2: Predict some of the experimental parameters

Parameter	Setting
Forecast basis	Radiance, air temperature, air pressure, humidity
MPA population	30
The maximum number of MPA iterations	30
MPA optimizes the upper boundary of the number of hidden cells	300
MPA optimizes the lower boundary of the number of hidden cells	50
MPA optimizes the upper bounding of the training cycle	300
MPA optimizes the lower boundary of the training cycle	50
MPA optimizes the upper bounds of learning rate	0.01
MPA optimizes the lower bound of the learning rate	0.001

5.1.2 Experimental Results

The prediction results of the VMD-MPA-LSTM method for photovoltaic power generation are illustrated in Fig. 5. To validate the applicability of the proposed approach, the experiment conducted forecasts across 83 time intervals, employing LSTM and VMD-LSTM as benchmark models for comparative analysis of prediction curves. The dataset features a temporal resolution of 1 h, comprising 295 time points in total. It includes meteorological parameters such as solar irradiance, ambient temperature, atmospheric pressure, and humidity, along with historical power data. After undergoing preprocessing steps including data cleaning, feature standardization, and sequence reconstruction, the dataset was chronologically partitioned with 70% allocated for training and 30% for testing. This partitioning strategy ensures no future information leakage during model training, thereby establishing a high-quality data foundation for the modeling process. As demonstrated, the proposed VMD-MPA-LSTM prediction method effectively forecasts distributed energy resource power output data, exhibiting superior performance in capturing dynamic generation patterns compared to conventional models.

To enhance the visual clarity of experimental results, a comparative analysis was conducted using LSTM, VMD-LSTM, VMD-SSA (Sparrow Search Algorithm)-LSTM, and the proposed VMD-MPA-LSTM methodologies. This comparative framework aims to underscore the advantages of our developed prediction approach. Performance evaluation was based on three key metrics: Root Mean Squared Error (RMSE), Mean Absolute Error (MAE), and Mean Absolute Percentage Error (MAPE). A detailed breakdown of the evaluation results is presented in Table 3, demonstrating that the proposed VMD-MPA-LSTM model exhibits superior predictive capabilities across all assessment criteria compared to the benchmark algorithms.

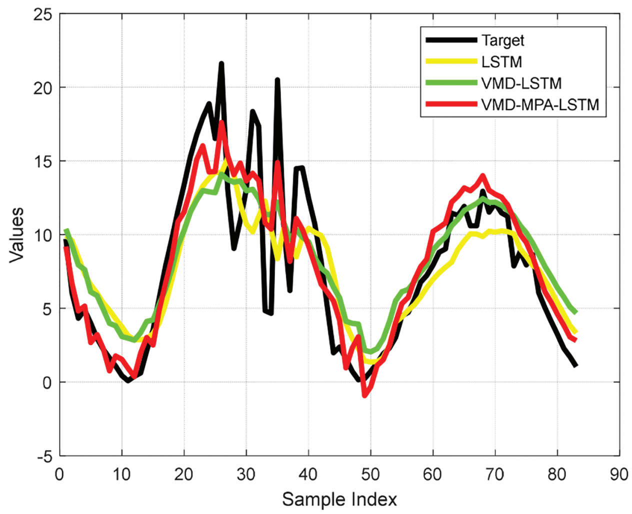

Figure 5: Distributed energy output forecast chart

Table 3: Predict some of the experimental data

The name of the method	Training set metrics			Test set metrics			Time (s)
	RMSE	MAE	MAPE	RMSE	MAE	MAPE	
LSTM	2.6348	2.1925	16.678%	3.3064	2.5811	26.8629%	4.4219
VMD_LSTM	2.2717	1.9491	14.319%	2.2718	1.9125	17.3324%	16.6866
VMD-SSA-LSTM	0.3906	0.3192	2.2712%	1.0003	0.8464	9.0028%	2986.5234
VMD-MPA-LSTM	0.3833	0.3129	2.2585%	1.0456	0.8926	9.2354%	2151.5362

As shown in Table 3, the VMD-MPA-LSTM prediction method demonstrates superior accuracy compared to LSTM and VMD-LSTM approaches, with the performance gap between VMD-MPA-LSTM and VMD-SSA-LSTM being negligible in terms of prediction accuracy. However, the VMD-MPA-LSTM method exhibits significantly enhanced computational efficiency, reducing calculation time by 834.9872 s relative to VMD-SSA-LSTM, thereby effectively minimizing computational complexity while achieving rapid prediction capabilities. This combination of high precision and operational speed underscores the proposed VMD-MPA-LSTM method's superiority in balancing forecasting accuracy and real-time performance, making it particularly advantageous for applications requiring both reliable energy output prediction and efficient computational resource utilization.

To validate the effectiveness of the prediction model under different starting points of the dataset, a multi-start rolling prediction method was adopted. The dataset was divided into three subsets (rows 1–120, rows 91–210, and rows 176–295, with each subset containing 120 data points) for experimental evaluation. The results are presented in Table 4.

The model demonstrates stable performance across test sets with varying data distributions and starting points. Particularly in Experiment 1 and Experiment 3, the VMD-MPA-LSTM model achieves comparable or even superior accuracy to the similarly-performing VMD-SSA-LSTM model, as evidenced by its lower RMSE and MAPE values in Experiment 3. This indicates that the model does not rely on specific data segments and possesses strong generalization capability, enabling it to adapt to different operating conditions.

Table 4: Comparison of multi-start prediction results

Experiment	The name of the method	Training set metrics			Test set metrics			Time (s)
		RMSE	MAE	MAPE	RMSE	MAE	MAPE	
1	LSTM	2.3129	1.8246	12.367%	2.063	1.6415	9.7885%	5.4387
	VMD_LSTM	1.7394	1.4395	10.108%	1.9784	1.6054	10.066%	23.1738
	VMD-SSA-LSTM	0.35084	0.25921	2.2827%	1.1796	0.98713	9.8017%	487.7528
	VMD-MPA-LSTM	0.3539	0.26028	2.3024%	1.0898	0.92836	9.1035%	2335.2850
2	LSTM	2.4791	1.9935	16.289%	2.6635	2.2225	21.171%	11.0892
	VMD_LSTM	1.8785	1.5694	13.098%	2.0011	1.6703	16.050%	22.6019
	VMD-SSA-LSTM	0.25483	0.19853	1.8401%	0.38369	0.33334	2.5134%	698.795535
	VMD-MPA-LSTM	0.25723	0.19223	1.8335%	0.33888	0.28837	2.0472%	1515.581
3	LSTM	3.1939	2.5816	24.54%	3.0605	2.6117	21.64%	3.9037
	VMD_LSTM	1.6519	1.3445	13.44%	2.4248	2.1634	18.73%	19.6511
	VMD-SSA-LSTM	0.46428	0.38733	3.7663%	1.9326	1.7978	19.2803%	1283.66107
	VMD-MPA-LSTM	0.44147	0.35908	3.612%	1.7765	1.6272	17.6762%	1409.253

In summary, the multi-start rolling prediction experiments fully validate the effectiveness, robustness, and superiority of the VMD-MPA-LSTM model for distributed energy output forecasting tasks. It not only significantly improves prediction accuracy but also demonstrates consistent generalization performance, thereby providing a fast and reliable data foundation for subsequent distribution network fault reconfiguration strategies.

5.2 Distribution Network Fault Reconstruction

In this paper, appropriate modifications are made to the IEEE 33-bus distribution network system by incorporating distributed generation equipment. This modified system is then used as a case study to analyze the fault restoration strategy proposed in this paper, which prioritizes the restoration of load sets over time.

5.2.1 Parameter Setting

The IEEE 33-bus system used in this paper is shown in Fig. 6, where the dashed lines represent standby tie lines.

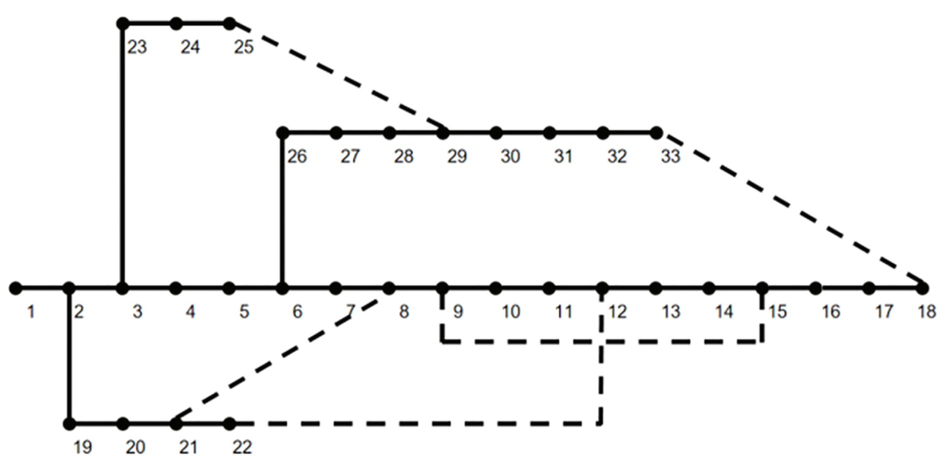

Figure 6: IEEE 33-bus distribution network

The computational setup, including solver parameters and Environment, is detailed in Tables 5 and 6.

Table 5: Computational setup

Category	Value
Solver	CPLEX
Absolute MIP gap tolerance	1.0
Big-M value	100
Big-M value	32.06
Number of nodes	33
Number of branches	37
Number of time periods	4
Total decision variables	~255

Table 6: Computational environment

Computational environment	MATLAB version	CPU model	JVM max memory	JVM allocated memory	Total execution time	Average time per period
PCWIN64	R2024a (24.1.0.2537033)	Intel(R) Core(TM) i7-10750H @ 2.60 GHz	1.5 GB	0.6 GB	10.34 s	2.58 s

The importance weights of the nodes are shown in Table 7, and the cost weights for nodes 2 to 33 at time point 1 are set as follows: [14; 18; 19; 16; 12; 9; 15; 100; 17; 13; 11; 100; 20; 8; 50; 50; 50; 7; 5; 10; 19; 6; 14; 16; 13; 50; 8; 11; 9; 100; 18; 14] (Unit: Ten Thousand Yuan).

Table 7: Setting of node importance weights

Importance level	Nodes	Weights
I	9,3,31	100
II	16,18,27	10
III	Else	1

In the fault reconfiguration model, black-start capability serves as a prerequisite for islanded operation. This capability enables distributed generators to self-start and establish stable operating conditions after complete grid voltage collapse. The optimization model ensures each island contains at least one black-start-capable power source through constraint formulation, thereby guaranteeing the restorability of outage areas.

This case study addresses post-fault emergency reconfiguration scenarios, whose technical objectives fundamentally differ from operational optimization. During fault reconfiguration, the system switches anti-islanding protection functions from preventive blocking in normal operation to supportive enabling for planned islands through preset control logic. This functional transition constitutes the technical prerequisite for implementing reconfiguration strategies rather than an optimization objective, thus ensuring the reliability and timeliness of post-fault power supply restoration. The status of distributed power sources is set as shown in Table 8. Due to the large fluctuations and poor stability in the output of distributed power sources without energy storage, they are not considered as supporting power sources for islanding in this paper for the time being. The total output of photovoltaic and wind power generation at each time point is shown in Fig. 7.

Table 8: Configuration parameters of distributed power sources

Energy type	Nodes	Capacity (MW)
Photovoltaic + Energy Storage	7	500
	13	300
Wind Power + Energy Storage	27	200
	17	300

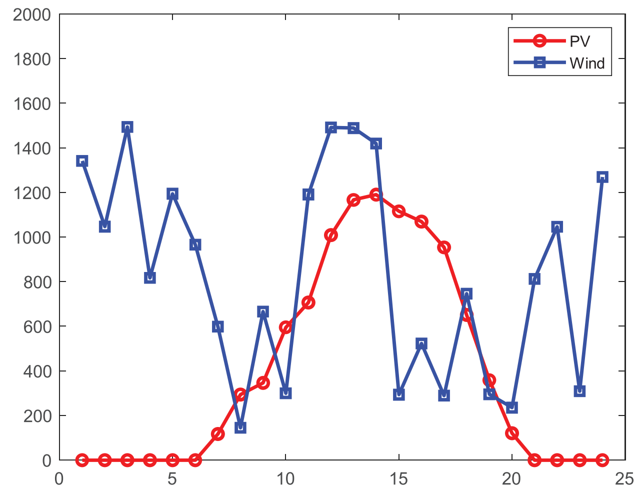

Figure 7: Schematic diagram of distributed power output and load power

Assuming that the model experiences a fault starting at 8 o'clock, with an additional faulty line occurring at 9 o'clock, and subsequently the fault is cleared and repaired by 10 o'clock. The faulty lines are shown in Table 9.

Table 9: Faulty line setting

Fault time	Faulty line
8:00	6, 14, 19, 25, 32
9:00	6, 14, 19, 21, 25, 32

5.2.2 Scheme Setting

To analyze the feasibility and superiority of the fault reconfiguration scheme for distribution networks proposed in this paper, which comprehensively considers both cost and power supply, four comparative schemes are proposed for the fault scenarios set up in this paper:

Scheme 1): When constructing the load priority restoration set, both cost factors and load importance factors are comprehensively considered. This is the scheme proposed in this paper.

Scheme 2): When constructing the load priority restoration set, cost factors are not considered, and only load importance factors are taken into account.

Scheme 3): When constructing the load priority restoration set, only cost factors are considered, and load importance factors are not taken into account [22].

Scheme 4): When constructing the load priority restoration set, both cost factors and load importance factors are compre-hensively considered. However, within the cost factors, the dynamic changes in cost are not taken into account.

5.2.3 Experimental Results and Analysis

The distribution network is set to experience a fault starting at 8:00 a.m. and is repaired by 10:00 a.m. At 8:00 and 9:00 a.m., after applying the fault reconfiguration strategy proposed in this paper, the reconfiguration results for these two time periods are shown in Fig. 8. It can be observed that the fault reconfiguration scheme proposed in this paper tends to prioritize the power supply to important nodes and nodes with higher outage costs. At 8:00 a.m., due to the relatively low photovoltaic power generation at this time, node 12 is directly disconnected, and a large number of nodes undergo load shedding to ensure power supply quality. At 9:00 a.m., both wind and photovoltaic power generation increase, so no nodes are disconnected in the distribution network, but load shedding is still required for multiple nodes. Since the time-varying load priority restoration set mentioned in this paper mainly targets changes in load outage losses after a fault persists for a period of time, the reconfiguration effects of the four schemes mentioned above during the 9:00 to 10:00 a.m. period are compared, and the results are shown in Table 10. It can be observed that, compared to Scheme 2 and Scheme 3, Scheme 1 proposed in this paper does not exhibit significant changes in the proportion of power supply restoration. This is determined by the total output of distributed generation at the time of the fault. Therefore, the main comparison focuses on two aspects: cost loss and the proportion of power supply to critical loads. Compared to Scheme 2, Scheme 1 incurs a total cost loss of only RMB 2,077,279, which is much less than the RMB 2,579,150 of Scheme 2, demonstrating a significant advantage in cost loss control. When compared to Scheme 3, which only considers cost loss, although Scheme 1 incurs a cost loss that is nearly RMB 130,000 more than Scheme 3, Scheme 3 fails to fully restore Class II loads. Therefore, Scheme 1 better meets the actual demands of power supply in distribution networks compared to Scheme 3. In Scheme 4, due to not considering the dynamic changes in cost loss, the cost loss of load interruption amounts to RMB 2,183,638, slightly higher than Scheme 1. This also verifies the necessity of constructing a dynamic load priority restoration set. A comprehensive comparison of the evaluation indicators for these four experimental schemes is presented in Table 11.

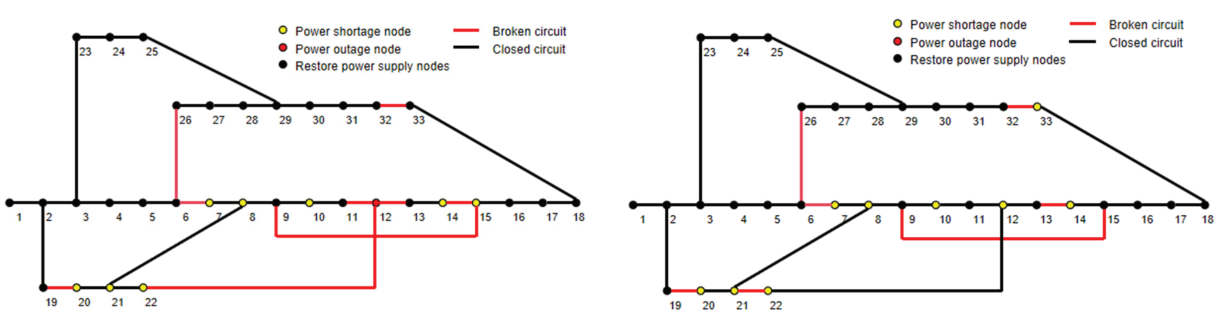

(a) 8:00–9:00 (b) 9:00–10:00

Figure 8: Diagram of distribution network fault reconfiguration results

Table 10: Islanded nodes after reconfiguration

Fault period	Island number	Nodes within the island
8:00–9:00	1	7, 8, 9, 10, 11, 20, 21, 22
	2	13, 14
	3	15, 16, 17, 18, 33
9:00–10:00	1(3 is merged into 1)	7, 8, 9, 10, 11, 12, 13, 20, 21, 22
	2	14, 15, 16, 17, 18, 33

Table 11: Comparison of experimental results

Experimental scheme	Load priority restoration set		Evaluation indicators			
	Whether cost is considered	Whether importance is considered	Proportion of power restoration	Total loss cost (Unit: ten thousand yuan)	Proportion of power restoration for Class I loads	Proportion of power restoration for Class II loads
1	Yes	Yes	64.48%	207.7279	100%	100%
2	No	Yes	64.50%	257.9150	100%	100%
3	Yes	No	64.40%	194.7424	100%	86.3%
4	Disregarding dynamic changes	Yes	64.47%	218.3638	100%	100%

Experimental results for different ratios of the β parameter are shown in Table 12 and Fig. 9.

Based on sensitivity analysis across multiple β ratio configurations, a clear trade-off relationship between load loss and cost loss has been revealed. As β_1 increases from 0.2 to 0.8, the system optimization mode gradually shifts from load-priority dominance to cost-optimization dominance, with the corresponding cost loss decreasing from 2.4686 million yuan to 2.0111 million yuan. Fig. 9 visually confirms this trend, clearly demonstrating the gradual reduction in economic losses as the optimization focus shifts toward cost efficiency. Comprehensive evaluation indicates that the balanced configuration scheme (β_1 = 0.5, β_2 = 0.5) achieves the optimal balance between load restoration and cost control. This configuration not only ensures continuous power supply to critical loads but also maintains operating costs within a reasonable range, thereby validating the critical role of weight parameters in multi-objective optimization coordination and their engineering applicability.

Table 12: Sensitivity analysis of the β parameter

Experimental scheme	Load priority restoration set		Evaluation indicators			
	Whether cost is considered	Whether importance is considered	Proportion of power restoration	Total loss cost (Unit: Ten Thousand Yuan)	Proportion of power restoration for Class I loads	Proportion of power restoration for Class II loads
1	0.2	0.8	64.53%	246.8620	100%	100%
2	0.4	0.6	64.51%	214.6725	100%	100%
3	0.5	0.5	64.48%	207.7279	100%	100%
4	0.6	0.4	64.49%	204.5728	100%	100%
5	0.8	0.2	64.42%	201.1123	100%	94.2%

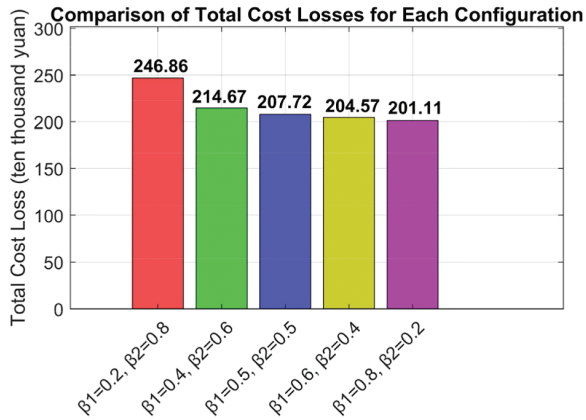

Figure 9: Comparison of total cost loss under different configurations

To further validate the sensitivity of the proposed reconfiguration strategy to the decay parameter γ, this paper conducts an experimental analysis on three configurations: $\gamma = 0.2$, $\gamma = 0.5$, and $\gamma = 0.8$, as shown in Fig. 10. The results indicate that the load loss patterns across four time periods remain entirely consistent under different γ values. The power supply restoration ratio for critical loads (Grade I and II) remains unaffected by variations in γ, consistently achieving 100%. Although the restoration sequence of non-critical loads exhibits minor fluctuations with changes in γ, the restoration priority based on load importance hierarchy remains stable. This demonstrates that the load priority restoration set constructed in this study possesses strong robustness to variations in the γ parameter, further confirming the reliability of the proposed strategy in practical engineering applications.

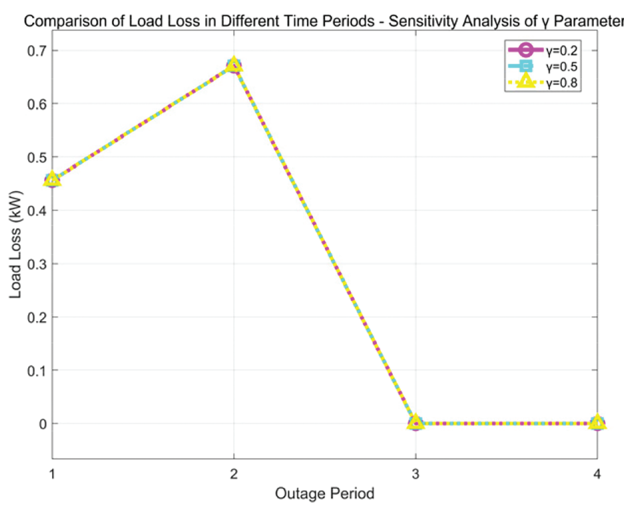

Figure 10: Comparison of load loss under different γ values

To verify the adaptability and scalability of the proposed fault reconfiguration strategy in more complex network structures, this section further conducts simulation experiments using the IEEE 69-node distribution network system as a case study. Compared to the 33-node system, the 69-node system features a more complex structure and a wider load distribution, which better reflects the typical characteristics of real-world distribution networks. This helps comprehensively evaluate the effectiveness and robustness of the proposed method.

Based on the experiments with the two starting time points of 8:00 and 11:00, a comparative experiment with a fault starting at 10:00 was added in this paper to further validate the adaptability of the parameter configuration β = 0.5 and γ = 0.2 during peak load periods. The experimental results are shown in Fig. 11.

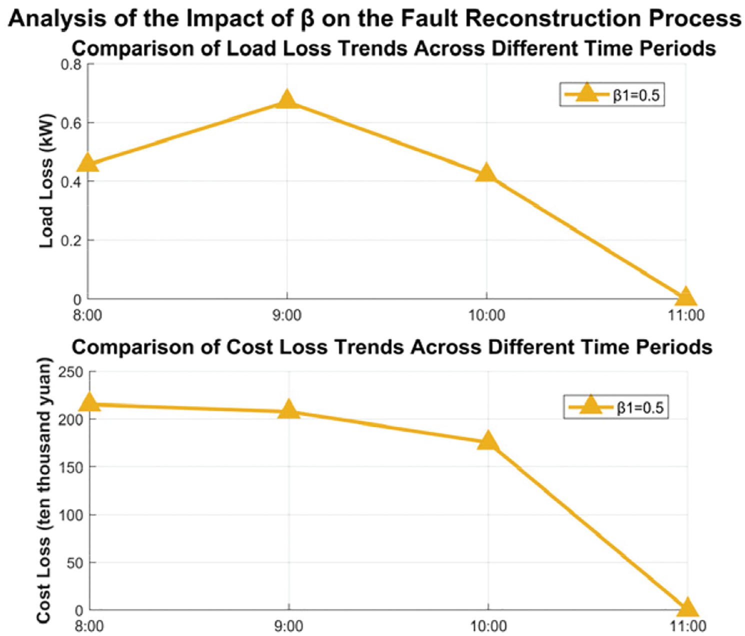

Figure 11: Analysis of the impact of β on the fault reconstruction process

Under the parameter settings of β = 0.5 and γ = 0.2, both load loss and cost loss during the fault reconstruction process exhibit significant time dependence. In terms of load loss trend, the system experiences relatively high load loss during the initial fault stage (8:00). As the reconstruction progresses, the load loss gradually decreases, showing a substantial reduction by 11:00, indicating that this parameter configuration demonstrates good dynamic adaptability in load recovery. Regarding cost loss, although some fluctuations occur between 9:00 and 10:00, the overall trend shows a decline, suggesting that this parameter combination effectively balances load importance and economic considerations. Overall, the configuration of β = 0.5 and γ = 0.2 achieves an effective trade-off between load recovery and economic costs during the fault reconstruction process, particularly demonstrating superior comprehensive performance in the later stages of reconstruction.

The IEEE 69-node system used in this study is illustrated in Fig. 12, where the dashed lines represent backup tie lines.

The importance weights of nodes are presented in Table 13.

Assuming that the model experiences a fault starting at 8 o'clock, with an additional faulty line occurring at 9 o'clock, and subsequently the fault is cleared and repaired by 10 o'clock. The faulty lines are shown in Table 14.

The distribution network experienced a fault starting at 8:00 and was fully restored by 10:00. The reconstruction results for the two time intervals (8:00 and 9:00) using the proposed distribution network reconfiguration strategy are shown in Fig. 13. To further analyze the impact of different weight configurations on the reconfiguration performance of the 69-node system, a sensitivity analysis of the β parameter is conducted, and the results are shown in Table 15.

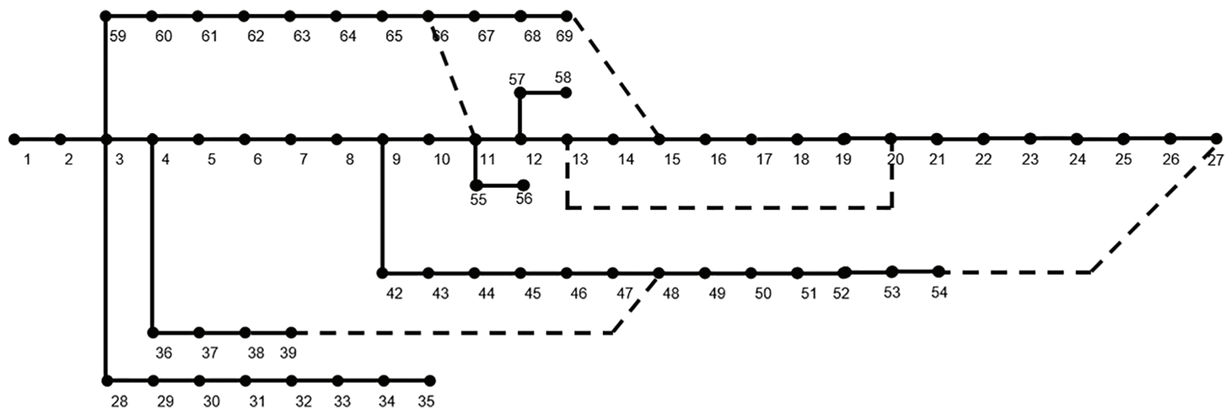

Figure 12: IEEE 69-bus distribution network

Table 13: Setting of node importance weights

Importance level	Nodes	Weights
I	9, 12, 31, 52	100
II	16, 18, 27, 45	10
III	Else	1

Table 14: Faulty line setting

Fault time	Faulty line
8:00	6, 14, 19, 25, 32, 45, 55
9:00	6, 14, 19, 21, 25, 32, 45, 55, 60

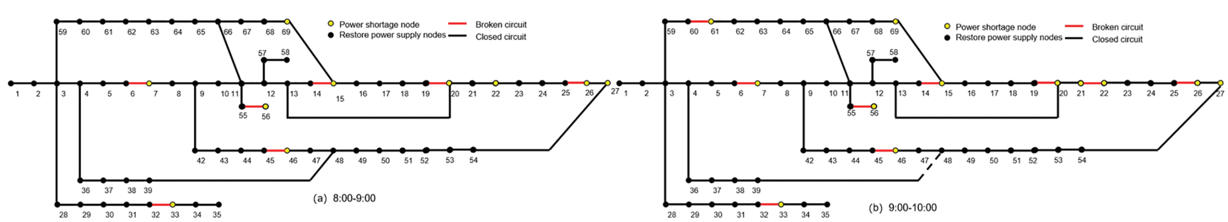

Figure 13: Diagram of distribution network fault reconfiguration results

Table 15: Sensitivity analysis of the β parameter

Experimental scheme	Load priority restoration set		Evaluation indicators			
	Whether cost is considered	Whether importance is considered	Proportion of power restoration	Total loss cost (Unit: Ten Thousand Yuan)	Proportion of power restoration for Class I loads	Proportion of power restoration for Class II loads
1	0.2	0.8	76.51%	375.67	100%	100%
2	0.4	0.6	76.52%	342.15	100%	100%
3	0.5	0.5	76.54%	328.72	100%	100%
4	0.6	0.4	76.49%	315.15	100%	100%
5	0.8	0.2	76.32%	307.21	100%	87.5%

A comprehensive analysis of the reconfiguration performance under different weight configurations during the 8:00–10:00 fault period demonstrates distinct trends in system performance. When $\beta_1 = 0.2$ and $\beta_2 = 0.8$, the system exhibits the highest total cost loss of 3.7567 million yuan, indicating that overemphasizing outage cost while neglecting load importance leads to increased overall losses during the initial fault stage. As β_1 progressively increases, the total cost shows a consistent downward trend. Specifically, during the 9:00–10:00 period, the configuration with $\beta_1 = 0.5$ and $\beta_2 = 0.5$ yields a total cost of 3.2872 million yuan, representing a relatively balanced operational state. When β_1 increases to 0.6 with $\beta_2 = 0.4$, the total cost further decreases to 3.1515 million yuan, establishing an optimized configuration. The lowest total cost of 3.0721 million yuan is achieved with $\beta_1 = 0.8$ and $\beta_2 = 0.2$, though this configuration may compromise power supply reliability for non-critical loads during periods of insufficient PV output at 8:00.

As illustrated in Table 13, maintaining the load importance weight β_1 within the 0.5 range throughout the fault period enables effective control of total cost while ensuring continuous power supply to critical loads. These results validate the rationality and practical effectiveness of the proposed fault reconfiguration strategy, which comprehensively considers both load importance and outage costs in coordinating multi-objective optimization.

6 Summary

This paper investigates the self-healing mechanism of novel distribution networks incorporating DG post-fault, initially employing the VMD-MPA-LSTM methodology to forecast DG power output in day-ahead scheduling, thereby providing real-time operational references for immediate distribution network response during contingencies. Subsequently, the study constructs time-varying load priority restoration sets by comprehensively evaluating load criticality and cost-based load interruption losses across different operational periods. Through systematic experimental validation, the following conclusions are derived: the proposed framework enables accurate DG output prediction to support rapid fault response, while the developed multi-criteria load restoration strategy optimizes recovery sequences by balancing operational priorities and economic factors, collectively enhancing the self-healing capability and resilience of modern distribution systems under distributed energy integration scenarios.

1) The proposed VMD-MPA-LSTM method enables fast and accurate prediction of distributed energy resource output, providing effective data support for the required distributed energy output parameters at the exact moment of system faults. This capability ensures real-time operational references for immediate fault response in modern distribution networks integrating distributed energy systems.
2) The proposed distribution network fault reconfiguration scheme, which integrates cost considerations with load criticality evaluation, enables effective post-fault network reconfiguration. Furthermore, the formulation of time-varying load priority restoration sets aligns with practical operational requirements, enhancing the applicability and real-world value of the proposed methodology.
3) Compared to traditional methods that solely prioritize load importance in constructing load priority restoration sets, the proposed scheme demonstrates superior cost control performance while simultaneously addressing the power supply demands of critical nodes, thereby offering enhanced practical applicability.

This paper primarily investigates distribution network fault restoration strategies that incorporate load interruption costs and load criticality considerations. For future research, it is recommended to explore more detailed aspects such as the economic impacts of network losses or investigate whether DG units without energy storage systems can effectively support the reconfiguration process of distribution networks under different operational scenarios.

Acknowledgement: The author obtained China Southern Power Grid Guangzhou Power Supply Bureau supports, and we sincerely appreciate this support.

Funding Statement: This research was supported by the Guangdong Power Grid Co., Ltd. Guangzhou Power Supply Bureau Science and Technology Innovation Technology Service Project (0301002024030103ZC00171).

Author Contributions: The authors confirm their contribution to the paper as follows: Conceptualization, Honglian Gao; Methodology, Honglian Gao; Data curation, Qingsong Zhang; Project administration, Qingsong Zhang; Investigation, Zeming Chen; Software, Lianchen Li; Supervision, Quanhui Liu; Validation, Quanhui Liu; Writing—original draft, Yuxiang Tian; Writing—review and editing, Xianfeng Xu. All authors reviewed and approved the final version of the manuscript.

Availability of Data and Materials: Not applicable.

Ethics Approval: Not applicable.

Conflicts of Interest: The authors declare no conflicts of interest.

References

1. Qi N, Cheng L, Tian LT, Guo JB, Huang RL, Wang CP. Review and prospect of distribution network planning research considering access of flexible load. Autom Electr Power Syst. 2020;44(10):193–207. (In Chinese). doi:10.1109/ei2.2018.8582294.
2. Wang JX, Luo XY, Yan L, Tang HG, Ma R. Identification technology of power-off event data quality in electricity acquisition system. J Electr Power Sci Technol. 2021;36(5):187–94. (In Chinese). doi:10.19781/j.issn.1673-9140.2021.05.023.
3. Ji BW, Wu ZA. Application of exponential smoothing method in load forecasting for power systems. Technol Innov Appl. 2018;8(30):173–4. (In Chinese).
4. Volkanovski A, Mavko B, Boševski T, Čauševski A, Čepin M. Genetic algorithm optimisation of the maintenance scheduling of generating units in a power system. Reliab Eng Syst Saf. 2008;93(6):779–89. doi:10.1016/j.ress.2007.03.027.
5. Tong Y, Yu L, Li S, Liu J, Qin H, Li W. Polynomial fitting algorithm based on neural network. ASP Trans Pattern Recognit Intell Syst. 2021;1(1):32–9. doi:10.52810/tpris.2021.100019.
6. Lu JX, Zhang QP, Yang ZH, Tu MF, Lu JJ, Peng H. Short-term load forecasting method based on CNN-LSTM hybrid neural network model. Autom Electr Power Syst. 2019;43(8):131–7. (In Chinese). doi:10.1109/pesgm40551.2019.8973549.
7. Pang CJ, Zhang B, Yu JM. Short-term power load forecasting based on LSTM recurrent neural network. Jiangsu Electr Eng. 2021;40(1):175–80,194. (In Chinese). doi:10.3390/en14102737.
8. Zhu J, Gu W, Jiang P, Wu Z, Yuan X, Nie Y. Integrated approach for optimal island partition and power dispatch. J Mod Power Syst Clean Energy. 2018;6(3):449–62. doi:10.1007/s40565-017-0314-z.
9. Liao F, Chen JR, Qu WC, Wang YQ, Hu YH, Wu N. Active distribution network recon-figuration based on an improved social spider algorithm. Proc CSU-EPSA. 2023;35(10):125–33.
10. Fu JW, Shi CK, Yin H, Guan SL, Wang AQ, Wang Y. Distribution network fault type identification method based on feature-summarizing matrix. Electr Power. 2021;54(11):125–32. (In Chinese). doi:10.11930/j.issn.1004-9649.202003220.
11. He LG, Wang YC, Wang TT, Ai XM, Tan HY, Ke FC, et al. A two-stage black-start restoration optimization method for a microgrid containing multi-type heterogeneous resources. Power Syst Prot Control. 2023;51(17):37–48. (In Chinese). doi:10.19783/j.cnki.pspc.230071.
12. Rahimipour Behbahani M, Jalilian A. Reconfiguration of harmonic polluted distribution network using modified discrete particle swarm optimization equipped with smart radial method. IET Gener Transm Distrib. 2023;17(11):2563–75. doi:10.1049/gtd2.12869.

13. Xu Y, Wu T, Hu P, Wang N. Fault recovery method for distributed distribution network based on island partition. J Electr Eng Technol. 2025;20(1):23–35. doi:10.1007/s42835-024-01952-2.
14. Liu M, Wu J, Zhang Q, Zheng H. Fault recovery of distribution network with distributed generation based on pigeon-inspired optimization algorithm. Electronics. 2024;13(5):886. doi:10.3390/electronics13050886.
15. Yang Z, Han J, Li L, Deng Y, Yang F, Lei Y, et al. Research of islanding operation and fault recovery strategies of distribution network considering uncertainty of new energy. Electronics. 2023;12(20):4230. doi:10.3390/electronics12204230.
16. Parihar SS, Malik N. Network reconfiguration in the presence of optimally integrated multiple distributed generation units in a radial distribution network. Eng Optim. 2024;56(5):679–99. doi:10.1080/0305215X.2023.2187790.
17. Samal P, Panigrahy D. Simultaneous feeder reconfiguration, DSTATCOM allocation, and sizing using seagull optimization algorithm in unbalanced radial distribution systems. Soft Comput. 2024;28(7):6403–21. doi:10.1007/s00500-023-09472-3.
18. Wang K, Kang L, Yang S. A coordination optimization method for load shedding considering distribution network reconfiguration. Energies. 2022;15(21):8178. doi:10.3390/en15218178.
19. Rahimipour Behbahani M, Jalilian A, Sheikhi Fini A. Reconfiguration of distribution network for improving power quality indexes with flexible lexicography method. Electr Power Syst Res. 2024;230:110172. doi:10.1016/j.epsr.2024.110172.
20. Parsadust H, Hajiabadi ME, Lotfi H, Yazdi SB, Baghishani V. Locating switches in distribution networks in order to eliminate peak load in energy management program. In: 2024 28th International Electrical Power Distribution Conference (EPDC); 2024 Apr 23–25; Zanjan, Iran. p. 1–7. doi:10.1109/EPDC62178.2024.10571749.
21. Zheng HB, Mo SQ, Du Q, Qin TF, Wang SS, Li Z. MPPT control strategy for photovoltaic energy storage system based on improved marine predator algorithm. China Meas Test Technol. 2025;51(9):148–57. (In Chinese). doi:10.11857/j.issn.1674-5124.2024120070.
22. Liu J, Luo HX, Zhang XH, Kuan X. Robust islanding strategy for active distribution net-work considering power outage losses and interruptible loads. J Electr Power Sci Technol. 2023;38(2):141–9.